$$\frac{\partial \phi}{\partial X} = +1 \quad (\text{for } 0 \le Y \le 1) \tag{6}$$

at the right one ($X = 1$). The dimensionless boundary condition for a exhaling top boundary ($Y = 1$) is:

$$\frac{\partial \phi}{\partial Y} = +1 \quad (\text{for } 0 \le X \le 1) \tag{7}$$

Dimensionless boundary condition for negligible flux or impermeability (wherever evoked) becomes:

$$\frac{\partial \phi}{\partial X} = 0 \quad (\text{for } 0 \le Y \le 1) \tag{8}$$

at any vertical boundary (either $X = 0$ or $X = 1$) or:

$$\frac{\partial \phi}{\partial Y} = 0 \quad (\text{for } 0 \le X \le 1) \tag{9}$$

for either bottom ($Y = 0$) or top boundary ($Y = 1$).

In view of Eq. (4), scale $\Delta C$ depends on Rn-222 exhalation rates $J_{Rn}$, which in turn depends on the phosphogypsum content of the material [11],[12]. The lack of information about $J_{Rn}$ does not prevent one from performing simulations. On the contrary, as discussed ahead, one may carry out numerical simulations to obtain $J_{Rn}$, thus characterizing a given exhaling phosphogypsum-bearing material.

## 3 Numerical method

Aiming at design, scale-up and/or optimization, one may rely on numerical simulation to reduce the number of tests, thus saving material and/or human resources. In order to yield detailed distributions of Rn-222 activity concentration, an existing academic simulator has been continuously adapted [13],[14]. Programmed in FORTRAN, such non-commercial simulation code has been successfully employed to investigate coupled heat and mass transfer problems in media partially or fully filled up with porous material [21]-[24].

Able to deal with time-dependent phenomena in two-dimensions, such simulator numerically solves coupled partial differential equations related to conservation principles (i.e., bulk mass, momentum, energy and species). In this work, the code was adjusted to simulate time-varying Rn-222 activity concentration in air (dimensionless formulation), in a square domain as previously described.

Following a finite-volume discretization method, governing equations are converted into an algebraic system, which is solved through tri-diagonal matrix algorithm (TDMA) [25]. Numerical simulations were performed on uniform orthogonal grids while under-relaxation factor was set at 0.9. For the sake of information (though not used in simulations here carried out), continuity and momentum equations are coupled in the code via SIMPLER algorithm while staggered grids are adopted in order to prevent pressure oscillations [25].

## 4 Results and discussion

By reminding that the bottom boundary (floor) is allegedly free from phosphogypsum, four distinct exhaling scenarios are investigated. As sketched in Fig. 3, differences between them refer to whether or not a given boundary contains phosphogypsum, thus leading to Rn-222 exhalation into the adjacent air.

| Exhaling scenario | Sketch |
|---|---|
| (*a*) Configuration "A": One vertical (left) exhaling boundary | 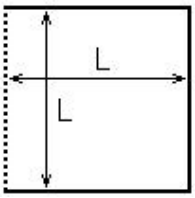 |
| (*b*) Configuration "B": Two vertical (left and right) exhaling boundaries | 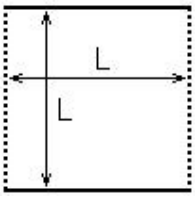 |
| (*c*) Configuration "C": One vertical (left) and one horizontal (top) exhaling boundaries | 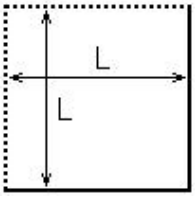 |
| (*d*) Configuration "D": Two vertical (left and right) and one horizontal (top) exhaling boundaries | 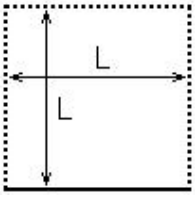 |

Fig. 3. Exhaling configurations simulated (solid line = impermeable or negligible-flux boundary; dashed line = uniform Rn-222 exhaling boundary).

Radon-222 self-decay constant is $\lambda = 2.098 \times 10^{-6}$ s$^{-1}$ whereas its diffusivity in open air has been reported as either $D = 1.2 \times 10^{-5}$ m$^2$·s$^{-1}$ [7] or $D = 1.1 \times 10^{-5}$ m$^2$·s$^{-1}$ [6],[18]. If $L = 3.5$ m is set as the characteristic length of the domain, the decay-to-diffusion ratio for scenarios simulated in this work results as $R \cong 2.3364$, according to Eq. (3).

### 4.1 Mesh sensitivity analysis

As far as the mesh size is concerned, a compromise between the number of grid points and numerical accuracy was examined by solving a steady-state simplification of Eq. (3), namely:

$$\frac{1}{R}\left(\frac{\partial^2\phi}{\partial X^2}+\frac{\partial^2\phi}{\partial Y^2}\right)-\phi=0 \qquad (10)$$

subjected to impermeable boundaries (i.e., to either $\partial\phi/\partial X = 0$ or $\partial\phi/\partial Y = 0$) except for the left vertical one (at $X = 0$), for which an exhaling condition is imposed (i.e., $\partial\phi/\partial X = -1$). In line with Fig. 3(*a*), such scenario is referred to as configuration "A".

The variation of the simulated value for $\phi$ at the midpoint $X = Y = 0.5$ as a function of the number $N$ of grid points along each coordinate $x$ and $y$ (so that the total number of points is $N \times N = N^2$) is shown in Fig. 4. As a compromise between convergence and computational effort, the 100×100 mesh was chosen for the subsequent sensitivity analysis with respect to the dimensionless advancing time step $\delta\tau$.

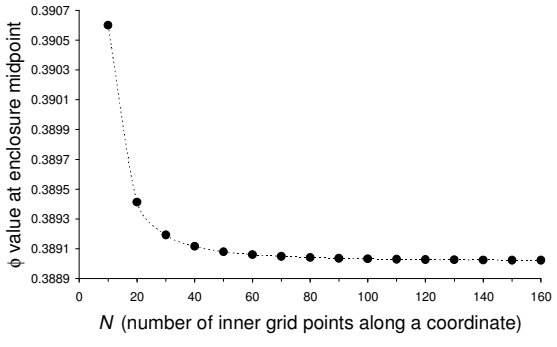


Fig. 4. Mesh sensitivity analysis with respect to grid spacing: $\phi$ simulated at the midpoint for different number of inner grid points (steady-state scenario).

In order to set $\delta\tau$ for time-varying simulations, the complete differential equation, Eq. (3), was solved for the same scenario (namely, configuration "A"), using the 100×100 mesh in the time interval $0 \le \tau \le 1$ (which refers to a simulated period of about $1/\lambda = 5.5$ days). The variation of value $\phi$ simulated at the midpoint and at the final instant $\tau = 1$ as a function of distinct $\delta\tau$ values is shown in Fig. 5. Again aiming at a compromise between accuracy and computational effort, $\delta\tau = 0.001$ was chosen so that numerical results shown hereafter were carried out using the 100×100 mesh and such advancing dimensionless time step.

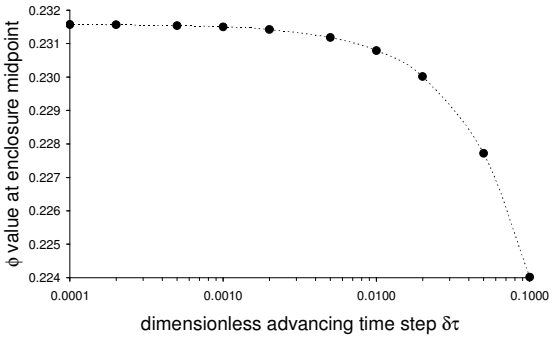


Fig. 5. Mesh sensitivity analysis with respect to advancing time steps: $\phi$ simulated at the midpoint at the final instant $\tau = 1$ (time-varying scenario).

### 4.2 Simulation of Rn-222 accumulation

Dimensionless Rn-222 activity concentration $\phi = \phi(X,Y,\tau)$ are numerically simulated for each exhaling scenario considered in this work (Fig. 3). Resulting concentration isolines at increasing dimensionless time instants are presented for configuration "A" in Fig. 6, configuration "B" in Fig. 7, configuration "C" in Fig. 8 and configuration "D" in Fig. 9. Time instants considered were $\tau = 0.25$, 0.50, 0.75 and 1.00 (which refer to approximately after 33 h, 66 h, 99 h and 132 h, respectively).

An interesting issue to ponder has to do with the location of the symmetry axis with reference to the $\phi$ distribution within the domain, for each exhaling configuration. As one would expect by examining the scenarios shown in Fig. 3, configuration "A" is symmetric about the horizontal axis through $Y = 0.5$, configuration "D" is symmetric about the vertical axis through $X = 0.5$ while those two symmetry axes are present in configuration "B". Configuration "C" is symmetric about the diagonal linking the upper left and lower right corners. It is worth noting that all those symmetry axes are retained throughout the time evolution of the concentration distribution. In other words, all time-dependent distributions retain their own symmetry patterns.

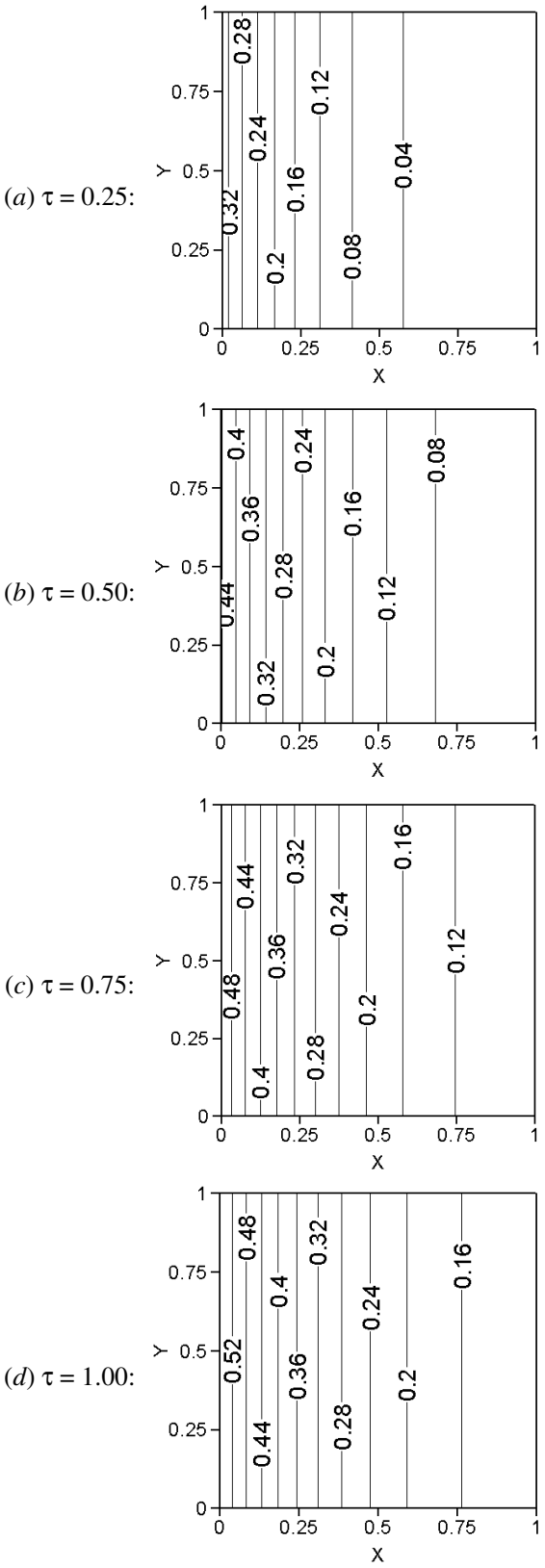


Fig. 6. Dimensionless Rn-222 concentration isolines simulated at increasing dimensionless time instants: exhaling configuration "A".

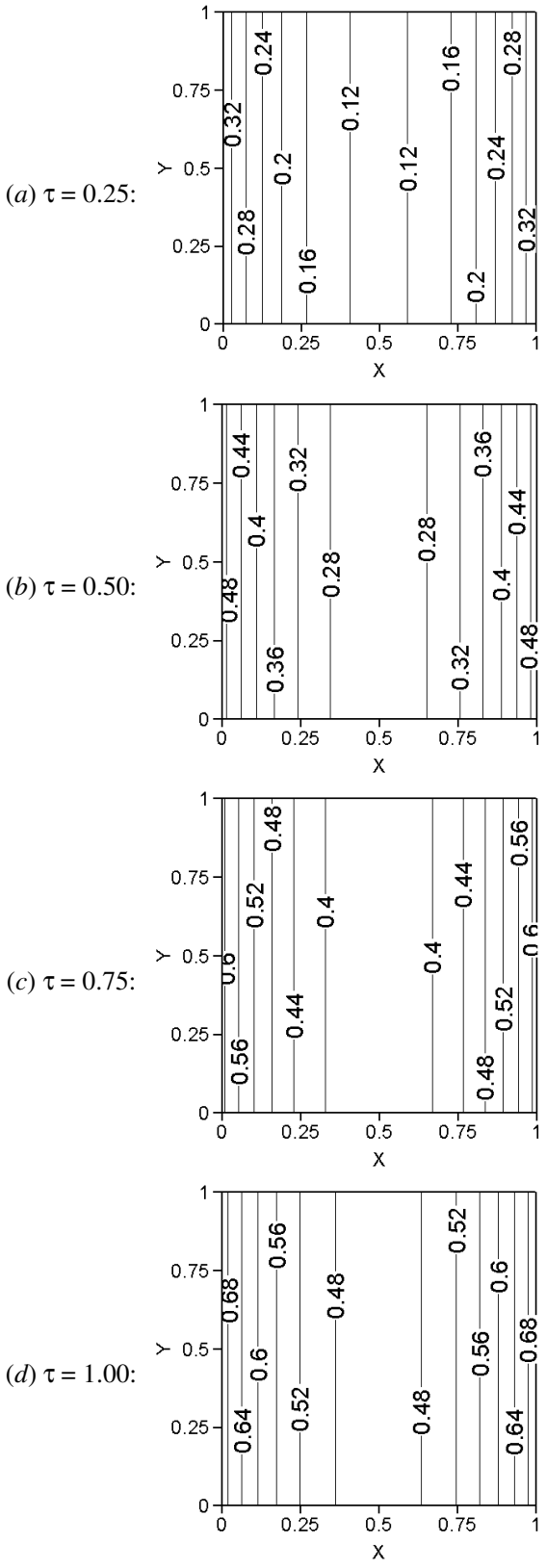


Fig. 7. Dimensionless Rn-222 concentration isolines simulated at increasing dimensionless time instants: exhaling configuration "B".

(*a*) $\tau = 0.25$:

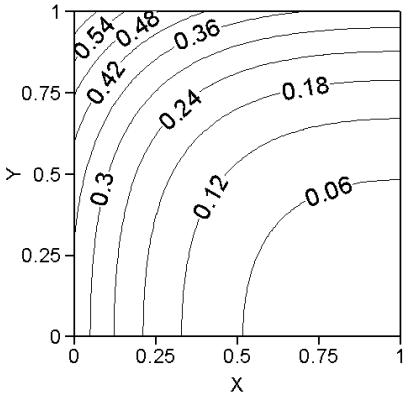


(*b*) $\tau = 0.50$:

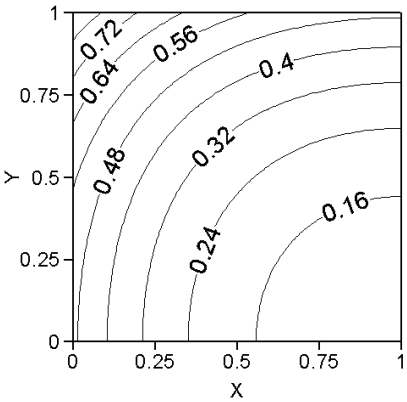


(*c*) $\tau = 0.75$:

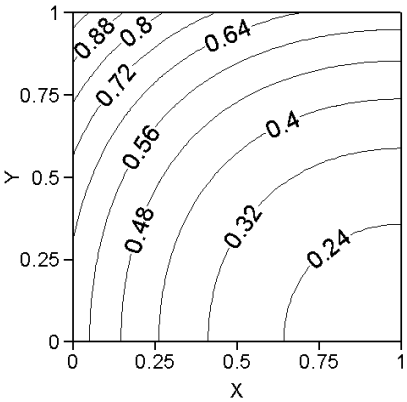


(*d*) $\tau = 1.00$:

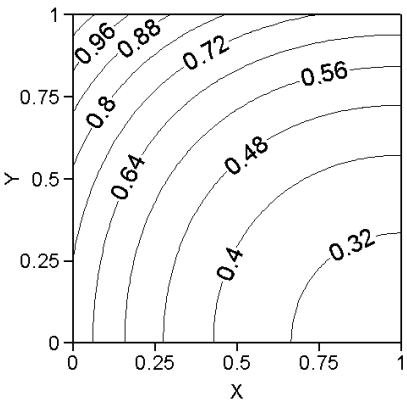


Fig. 8. Dimensionless Rn-222 concentration isolines simulated at increasing dimensionless time instants: exhaling configuration “C”.

(*a*) $\tau = 0.25$:

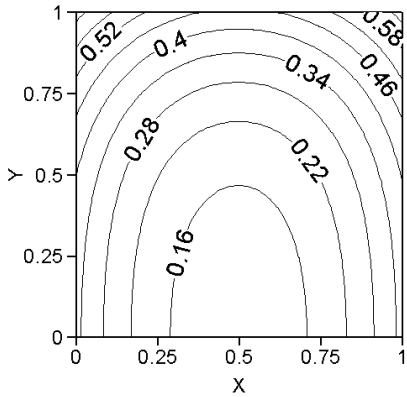


(*b*) $\tau = 0.50$:

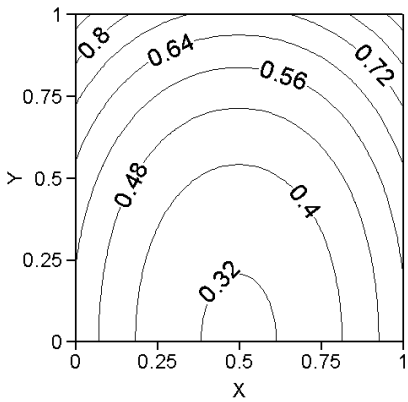


(*c*) $\tau = 0.75$:

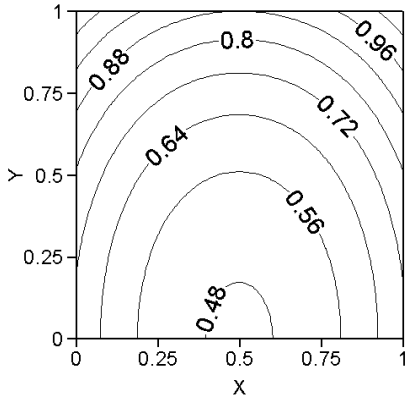


(*d*) $\tau = 1.00$:

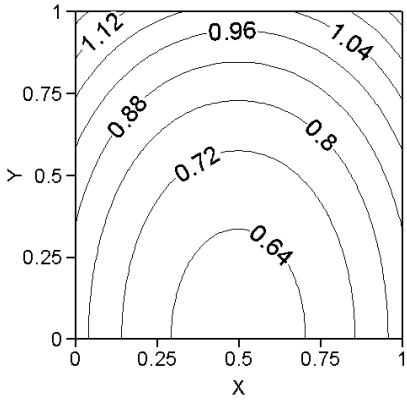


Fig. 9. Dimensionless Rn-222 concentration isolines simulated at increasing dimensionless time instants: exhaling configuration “D”.

It is also important to note that no homogeneous Rn-222 distribution is verified whatsoever inside the solution domain. As dimensionless time advances, increasing concentration levels are obtained since no air exchange mechanism is accounted for in the model. Such fact explains why air renewal is indeed necessary to make a dwelling habitable by humans and acceptable according to Rn-222 standards.

The dimensionless time range here considered ($0 \leq \tau \leq 1$) was not long enough for steady-state to be reached by any exhaling scenario. In view of Eq. (3) or (10), steady-state is reached as soon as $\partial^2\phi/\partial X^2 + \partial^2\phi/\partial Y^2. = R\cdot\phi$, throughout the solution domain.

One may use numerical simulations as means to characterize phosphogypsum-bearing materials with respect to Rn-222 exhalation rates. For instance, by evoking the proportionality between $\phi$ and $C$ as given by Eq. (2), one may estimate scale $\Delta C_{est}$ by fitting numerically simulated values $\phi_{num}$ for the dimensionless Rn-222 activity concentration at a particular position (e.g., midpoint of the solution domain) against experimentally measured values $C_{exp}$ for Rn-222 activity concentration at the same position (e.g., midpoint of a geometrically similar prototype). One may then manipulate Eq. (2) in order to obtain:

$$\phi = \frac{C - C_0}{\Delta C} \quad \Rightarrow \quad \Delta C_{est} = \frac{C_{exp} - C_0}{\phi_{num}} \qquad (11)$$

Once scale $\Delta C_{est}$ is known together with Rn-222 diffusivity $D$ and characteristic length $L$, one may estimate related Rn-222 exhalation rates $J_{Rn,est}$ with the help of Eq. (4), namely:

$$\Delta C = \frac{J_{Rn} L}{D} \quad \Rightarrow \quad J_{Rn,est} = \frac{\Delta C_{est} D}{L} \qquad (12)$$

As already pointed out, Rn-222 exhalation rates are key parameters for radiological protection design and/or radiation exposure assessment. For the sake of comparison, those rates from phosphogypsum-bearing walls have been reported to range as $0.0014 \leq J_{Rn} \leq 0.0111$ Bq·m$^{-2}$·s$^{-1}$ [9].

At this point, one should remember that $C_0 = 0$ was assumed in the present model. Whenever $C_{0,exp} \neq 0$, such non-zero initial concentration prevailing in the closed room (chamber) should be experimentally measured to be properly introduced in Eq. (11). Again for comparison purposes, outdoor air-borne Rn-222 activity concentration have been measured as approximately 10 Bq·m$^{-3}$ [6].

It is worth recalling that air was here assumed to be isothermal and motionless so that thermal effects and convective (mass and/or energy) transfers were disregarded. Otherwise, continuity, momentum and energy equations should be evoked in the model and numerically solved while Rn-222 activity (species) equation should be extended so as to accommodate those additional phenomena. Such comprehensive approach is left for forthcoming developments of this work.

Indeed, other effects include not only convective transport due to air motion (related to the existence of fans, doors and/or windows) but also the presence of the phosphogypsum-bearing material itself in the solution domain (which can be extended up to two or even three dimensions). The nuclear physicist or engineer should evoke numerical methods to solve the resulting partial differential equation system.

# 4 Concluding remarks

Aiming at large-scale (and commercial) exploitation of phosphogypsum as alternative building material, knowledge of Rn-222 exhalation and accumulation in indoor air is fundamental for proper radiological protection design. Zero-order model frameworks with respect to spatial coordinates have been used to simulate time-dependent Rn-222 concentration in indoor air. In those models, uniform Rn-222 activity distribution is supposed throughout the domain of interest. Nevertheless, such hypothesis breaks down if point-to-point variation is desired.

Accordingly, the present work proposed a time-varying second-order model for Rn-222 activity concentration, which was implemented by adapting an existing academic (i.e., non-commercial) finite-volume simulator for transport phenomena in porous media. Numerical simulations were carried out for a square domain subjected to four distinct diffusion-dominant Rn-222 exhaling scenarios.

While expected symmetries were retained during the time evolution of Rn-222 activity distributions in simulated scenarios, numerical results confirmed that no homogeneous distribution occurs inside the solution domain. As Rn-222 activity concentrations were observed to be particularly higher near upper corners, one may overestimate activity levels (in comparison to average levels) if recordings are only accomplished in the vicinity of those corners.

Having in mind the ability to deal with more general situations, a primary objective is to widen the model framework in order to include additional phenomena (e.g., thermal effects and/or convective heat/mass transfer) while being extended to three-dimensional solution domains. The academic finite-

volume simulator must be properly adapted as well in order to cope with those model extensions.

*Nomenclature*

| | |
|---|---|
| $C$ | Rn-222 activity concentration ($Bq \cdot m^{-3}$) |
| $D$ | Rn-222 diffusivity in open air ($m^2 \cdot s^{-1}$) |
| $J$ | Rn-222 flux / exhalation ($Bq \cdot m^{-2} \cdot s^{-1}$) |
| $L$ | Characteristic length of solution domain (m) |
| $N$ | Number of inner grid points (dimensionless) |
| $R$ | Decay-to-diffusion ratio (dimensionless) |
| $t$ | Time (s) |
| $X$, $Y$ | Cartesian coordinates (dimensionless) |
| $x$, $y$ | Cartesian coordinates (m) |
| $x_c$ | Thickness of phosphogypsum material (m) |

*Greek symbols*

| | |
|---|---|
| $\lambda$ | Rn-222 decay constant ($s^{-1}$) |
| $\tau$ | Time (dimensionless) |
| $\phi$ | Rn-222 activity concentration (dimensionless) |
| $\Delta C$ | Rn-222 activity concentration scale ($Bq \cdot m^{-3}$) |
| $\delta\tau$ | Advancing time step (dimensionless) |

*Subscripts and superscripts*

| | |
|---|---|
| est | Estimated (assessed) value |
| exp | Experimentally measured value |
| num | Numerically simulated value |
| Rn | Absolute value for Rn-222 flux / exhalation |
| $x$, $y$ | Directions along Cartesian coordinates |
| 0 | Initial value for Rn-222 activity concentration |

*References:*


[1] Rutherford P.M., Dudas M.J., Samek R.A., Environmental impacts of phosphogypsum, *Science of the Total Environment*, vol. 149, 1994, pp. 1-38.

[2] Mazzilli B., Palmiro V., Saueia C., Nisti, M.B., Radiochemical characterization of Brazilian phosphogypsum, *Journal of Environmental Radioactivity*, vol. 49, 2000, pp. 113-122.

[3] Nero A.V., Radon and its decay products in indoor air: an overview, In: *Radon and its Decay Products in Indoor Air*, Nazaroff W.W., Nero A.V. (editors), John Wiley & Sons, 1988.

[4] James A.C., Lung dosimetry, In: *Radon and its Decay Products in Indoor Air*, Nazaroff W.W., Nero A.V. (editors), John Wiley & Sons, 1988.

[5] Cross F.T., Evidence of lung cancer from animal studies, In: *Radon and its Decay Products in Indoor Air*, Nazaroff W.W., Nero A.V. (editors), John Wiley & Sons, 1988.

[6] United Nations Scientific Committee on the Effects of Atomic Radiation, *Sources and Effects of Ionizing Radiation*, 2000.

[7] Nazaroff, W.W., Moed B.A., Sextro R.G., Soil as a source of indoor radon: generation, migration and entry, In: *Radon and its Decay Products in Indoor Air*, Nazaroff W.W., Nero A.V. (editors), John Wiley & Sons, 1988.

[8] Nazaroff W.W., Radon transport from soil to air, *Reviews of Geophysics*, vol. 30, 1992, pp. 137-160.

[9] Stranden E., Building materials as a source of indoor radon, In: *Radon and its Decay Products in Indoor Air*, Nazaroff W.W., Nero A.V. (editors), John Wiley & Sons, 1988.

[10] Nazaroff W.W., Teichman K., Indoor radon: exploring US federal policy for controlling human exposures, *Environmental Science and Technology*, vol. 24, 1990, pp. 774-782.

[11] Jang M., Kang C.S., Moonet J.H., Estimation of Rn-222 release from the phosphogypsum board used in housing panels, *Journal of Environmental Radioactivity*, vol. 80, 2005, pp. 153-160.

[12] Rabi J.A., Silva N.C., Radon exhalation from phosphogypsum building boards: symmetry constraints, impermeable boundary conditions and numerical simulation of a test case, *Journal of Environmental Radioactivity*, vol. 86, 2006, pp. 164-175.

[13] Rabi J.A., Mohamad A.A., Radon-222 exhalation rates from phosphogypsum-bearing embankment subjected to constant temperature and fixed activity concentration, *Journal of Porous Media*, vol. 8, 2005, pp. 175-191.

[14] Rabi J.A., Mohamad A.A., Parametric modelling and numerical simulation of natural-convective transport of radon-222 from a phosphogypsum stack into open air, *Applied Mathematical Modelling*, vol. 30, 2006, pp. 1546-1560.

[15] Stranden E., Berteig L., Radon in dwellings and influencing factors, *Health Physics*, vol. 39, 1980, pp. 275-284.

[16] Edwards J.C., Bates R.C., Theoretical evaluation of radon emanation under a variety of conditions, *Health Physics*, vol. 39, 1980, pp. 263 -274.

[17] Loureiro C.O., *Simulation of the steady-state transport of radon from soil into houses with basements under constant negative pressure*, Ph.D. thesis, University of Michigan, USA, 1987.

[18] Yu C., Loureiro C.O., Cheng J.J., Jones L.G., Wang Y.Y., Chia Y.P., Faillace E., *Data Collection Handbook to Support Modeling Impacts of Radioactive Materials in Soil*, Argonne National Laboratory, USA, 1993.

[19] Andersen C.E., *Radon transport modelling: user's guide to RnMod3d*, Riso-R-1201(EN), Riso National Laboratory, Denmark, 2000.

[20] Riley W.J., Robinson A.L., Gadgil A.J., Nazaroff W.W., Effects of variable wind speed and direction on radon transport from soil into buildings: model development and exploratory results, *Atmospheric Environment*, vol. 33, 1999, pp. 2157-2168.

[21] Mohamad A.A., Bennacer R., Natural convection in a confined saturated porous medium with horizontal temperature and vertical solutal gradients, *International Journal of Thermal Sciences*, vol. 40, 2001, pp. 82-93.

[22] Mohamad A.A., Bennacer R., Double diffusion, natural convection in an enclosure filled with saturated porous medium subjected to cross gradients; stably stratified fluid, *International Journal of Heat and Mass Transfer*, vol. 45, 2002, pp. 3725-3740.

[23] Bennacer R., Beji H., Mohamad A.A., Double diffusive convection in a vertical enclosure inserted with two saturated porous layers confining a fluid layer, *International Journal of Thermal Sciences*, vol. 42, 2003, pp.141-151.

[24] Mohamad A.A., Heat transfer enhancements in heat exchangers fitted with porous media. Part I: constant wall temperature, *International Journal of Thermal Sciences*, vol. 42, 2003, pp. 385-395.

[25] Patankar S.V., *Numerical Heat Transfer and Fluid Flow*, Hemisphere, 1980.